Aerodynamic Noise Prediction for Long-Span Bodies

J. H. Seo*, K. W. Chang†, and Y. J. Moon‡
Department of Mechanical Engineering, Korea University, Seoul, 136-701, Korea

An aerodynamic noise prediction method for long-span bodies is proposed. The present method consists of (i) incompressible large eddy simulation (LES), (ii) linearized perturbed compressible equations (LPCE) for a 2D acoustic field at zero spanwise wave number, k_z=0, (iii) 2D Kirchhoff method and then Oberai's 3D-correction for the spectral acoustic pressure in the far-field, and finally (iv) estimation of the far-field sound pressure level (SPL) for the long span. In the present study, accuracy of the present method is assessed for a broadened tone as well as the broadband noise generated by a flow (Re_D=4.6×10^4 and M=0.21) past a circular cylinder with 30D span. Aerodynamic and aeroacoustic results are very closely compared with the experimentally measured data. Also, the numerical issues on LES, LPCE, and prediction method for the far-field SPL for long span are discussed in conjunction with the flow physics.

I. Introduction

Turbulent flows around long-span bodies (e.g. circular cylinder, airfoil, flat plate, and forward/backward steps) are often encountered in aerodynamics. Although turbulence characteristics of the flow have extensively been studied by direct numerical simulation (DNS) or large eddy simulation (LES), its noise prediction is not a simple matter, especially at low Mach numbers. At low Mach numbers, a scale disparity between the turbulent eddy size and the acoustic wave length is so large that direct computation of the turbulent flow noise is very expensive and difficult.

In this regard, many researchers have used hybrid methods. The Lighthill/Curle integral formulation with compressible or incompressible LES solution[1,2] has widely been used. The linearized Euler equations (LEE) with the source terms extracted form the LES solutions have also been developed[3-5]. This method is shown to be effective but defining the source terms still remains as an open issue. Recently, Ewert and Schröder proposed the acoustic perturbation equations (APE)[6], which is based on source-term filtering for the compressible LES solution. This method has been exercised with a turbulence trailing-edge noise problem[7].

In this study, we propose a hybrid method for the prediction of a low Mach number turbulent flow noise for long span. This method is based on a hydrodynamic/acoustic splitting technique[8-13], an alternative to solve the low Mach number aeroacoustics. A turbulent flow is computed by incompressible LES, while the generation and propagation of the acoustic field is predicted by the linearized perturbed compressible equations (LPCE)[14], with the acoustic sources acquired from the incompressible LES solution. This method ensures consistent, grid-independent acoustic solutions by suppressing the unstable vortical mode in the perturbed system. The present method is computationally efficient at low Mach numbers because it is based on an incompressible flow solver and the grid systems for flow and acoustics can be treated separately.

The far-field sound for the long span is then calculated by an approximate but efficient computational approach: (i) a two-dimensional acoustic pressure in the near- and mid-field is calculate4d by LPCE with the spanwise-integrated incompressible LES solution, (ii) the far-field acoustic pressure is obtained by extrapolating the mid-field solution with the Kirchhoff method, (iii) a three-dimensional correction is then made by Oberai's formula, and (iv) finally, the sound pressure level for the simulated span is corrected to that for the long span, considering the spanwise coherence function of the acoustic pressure emitted from each subsection of the body distributed in the spanwise direction. In this study, the final step (iv) is formally derived, revisiting the previous works of Kato et al. [21] and Perot et al. [2], and discussion is made for the relations between the spanwise coherence function of the acoustic pressure and that of the surface pressure.

* Ph.D. candidate, AIAA student member.
† Graduate student, AIAA student member.
‡ Professor, AIAA senior member, corresponding author (yjmoon@korea.ac.kr)

In the present study, the afore-mentioned computational methods are validated for a broadened tone as well as the broadband noise generated by a flow at Re_D=4.6×10^4 and M=0.21 past a circular cylinder with 30D span. The computed aerodynamic and aeroacoustic results are compared with the experimentally measured data[23,26] and the numerical issues on LES, LPCE, and prediction methods for the far-field SPL for long span are discussed in conjunction with the flow physics.

II. Computational Methodologies

A. Incompressible LES/LPCE Hybrid Method

An aerodynamic noise prediction for long span bodies starts with a computation of low Mach number turbulent flow by incompressible LES. This is based on a hydrodynamic/acoustic splitting method, in which the total flow variables are decomposed into the incompressible and perturbed compressible variables as,

$$\begin{aligned} \rho(\vec{x},t) &= \rho_0 + \rho'(\vec{x},t) \\ \vec{u}(\vec{x},t) &= \vec{U}(\vec{x},t) + \vec{u}'(\vec{x},t) \\ p(\vec{x},t) &= P(\vec{x},t) + p'(\vec{x},t) \end{aligned} \quad (1)$$

The incompressible variables represent hydrodynamic turbulent flow field, while acoustic fluctuations and other compressibility effects are resolved by perturbed quantities denoted by ($'$) .

The incompressible LES equations are the filtered incompressible Navier-Stokes equations written as

$$\frac{\partial \tilde{U}_j}{\partial x_j} = 0 \quad (2)$$

$$\rho_0 \frac{\partial \tilde{U}_i}{\partial t} + \rho_0 \frac{\partial}{\partial x_j}(\tilde{U}_i \tilde{U}_j) = -\frac{\partial \tilde{P}}{\partial x_i} + \mu_0 \frac{\partial}{\partial x_j}\left(\frac{\partial \tilde{U}_i}{\partial x_j} + \frac{\partial \tilde{U}_j}{\partial x_i}\right) - \rho_0 \frac{\partial}{\partial x_j} M_{ij}, \quad (3)$$

where the resolved quantities are denoted by ($\tilde{}$) and the unknown sub-grid tensor M_{ij} is modeled as

$$M_{ij} = \widetilde{U_i U_j} - \tilde{U}_i \tilde{U}_j = -(C_s \Delta)^2 \left|\tilde{S}\right| \tilde{S}_{ij}. \quad (4)$$

Here, Δ is the mean radius of a grid cell (computed as the cubic root of its volume). For solving the filtered incompressible Navier-Stokes equations, an iterative fractional-step method is used. The governing equations are spatially discretized with a sixth-order compact scheme[15] to avoid excessive numerical dissipations and dispersions errors and integrated in time by a four-stage Runge-Kutta method. The 10th-order spatial filtering of Gaitonde et al.[16] is also applied to enhance the numerical stability with high frequency cutoff.

To calculate the perturbed quantities, the perturbed compressible equations (PCE)[13] are derived by subtracting the incompressible Navier-Stokes equations from the compressible ones. The PCE, however, exhibits self-excited errors by instability of the perturbed vorticity ($\vec{\omega}' = \nabla \times \vec{u}'$), if $\vec{\omega}'$ is not properly resolved with the acoustic grid. This is even more pronounced at high Reynolds numbers[14]. Thereby, present authors have proposed the linearized perturbed compressible equations (LPCE), in which evolution of the perturbed vorticity is pre-suppressed in the formulation, deliberating the fact that perturbed vorticity has a little effect on the noise generation at low Mach numbers. A set of LPCE can be written in a vector form as,

$$\frac{\partial \rho'}{\partial t} + (\vec{U} \cdot \nabla)\rho' + \rho_0 (\nabla \cdot \vec{u}') = 0 \quad (5)$$

$$\frac{\partial \vec{u}'}{\partial t} + \nabla(\vec{u}' \cdot \vec{U}) + \frac{1}{\rho_0} \nabla p' = 0 \quad (6)$$

$$\frac{\partial p'}{\partial t} + (\vec{U}\cdot\nabla)p' + \gamma P(\nabla\cdot\vec{u}') + (\vec{u}'\cdot\nabla)P = -\frac{DP}{Dt}. \tag{7}$$

The LPCE is linearized to a base incompressible flow field and its formulation is much simpler than the original PCE. Because the curl of linearized perturbed momentum equations, Eq. (6) yields

$$\frac{\partial \vec{\omega}'}{\partial t} = 0, \tag{8}$$

LPCE consequently prevents any further changes (generation, convection, and decaying) of perturbed vorticity in time. It also provides a physical base for using large grid spacing near the wall because they are in an invisicd form. Details on derivation of LPCE and characteristics of the perturbed vorticity can be found in reference[14]. The LPCE has been validated for a laminar tone prediction for a circular cylinder at M=0.1 and also for vortex sound problems at high Reynolds numbers – quadruple sound of Kirchhoff vortex and temporal mixing layer noise[14].

The left hand side of LPCE represents effects of acoustic wave propagation and refraction in an unsteady, inhomogeneous flow, while the right hand side only contains the acoustic source term, projected from the hydrodynamic flow solution. For low Mach number flows, it is interesting to note that the total change of hydrodynamic pressure, *DP/Dt* is only considered as the explicit noise source term. The turbulent flow fluctuations are represented by the static pressure field in incompressible LES solutions and their noise can be calculated by LPCE through the material derivatives of this pressure field. Therefore, LPCE excludes any uncertainty in modeling the source terms for the turbulence-generated noise.

B. Acoustic Field Computation

In LES, a spanwise periodic boundary condition allows us to capture the spanwise-correlated flow structure with a span, L_s, relatively short but large enough to include the turbulence correlation length, L_c. In acoustic calculation, however, applying a periodic boundary condition for the same span yields an unphysically correlated acoustic result[2,7,17], because acoustic length scale is usually much larger than the turbulence length scale at low Mach numbers. To avoid this matter, one must either use a very long span that fully covers the acoustic correlation length $l'_c (>> L_c)$ or apply an absorbing boundary condition at the spanwise boundaries (i.e. different boundary conditions are employed for the flow and acoustics). Both approaches are difficult to be achieved but it must be pointed out that the latter could be an easy task for the present hybrid method.

In this study, an approximated but efficient method is pursued. Instead of computing a three-dimensional acoustic field[18], a two-dimensional field of acoustics is calculated in the mid-span plane with acoustic sources evaluated at the zero spanwise wave number, k_z=0 (i.e. integrated in the spanwise direction) and then it is corrected to the three-dimensionally radiated one. Considering an acoustic wave equation which is Fourier-transformed in the spanwise direction, a three-dimensionally radiated acoustic pressure in the mid-span plane (i.e. at z=0), $\hat{p}'_{3D}$ is related to a two-dimensionally predicted acoustic pressure at k_z=0, $\hat{p}'_{2D}$ by

$$\hat{p}'_{3D}(r,\theta,0,\omega) \approx \hat{p}'_{2D}(r,\theta,\omega)\frac{1+i}{2}\sqrt{\frac{\omega}{c_0\pi r}}, \tag{9}$$

where c_o is the ambient speed of sound. Derivation of this relation proposed by Oberai et al. can be found in reference[19]. This is approximately equivalent to a 3D computation of the acoustic field with an absorbing spanwise boundary condition and can be employed for most of the long-span bodies[7].

At low Mach numbers, acoustic computational domain is often truncated in the mid-field, due to the lack of computational resources. If an observer's position (or measurement point in experiment) is very far from the source, acoustic pressure calculated by LPCE can be extrapolated by a Kirchhoff method. The 2D Kirchhoff method in frequency domain[20] is given by

$$4i\,\hat{p}' = -\int_S \left[\frac{\partial \hat{p}'}{\partial n}H_0^{(2)}(\omega r/c_0) - \frac{\omega}{c_0}(\hat{n}\cdot\hat{r})\hat{p}'H_1^{(2)}(\omega r/c_0)\right]dS, \tag{10}$$

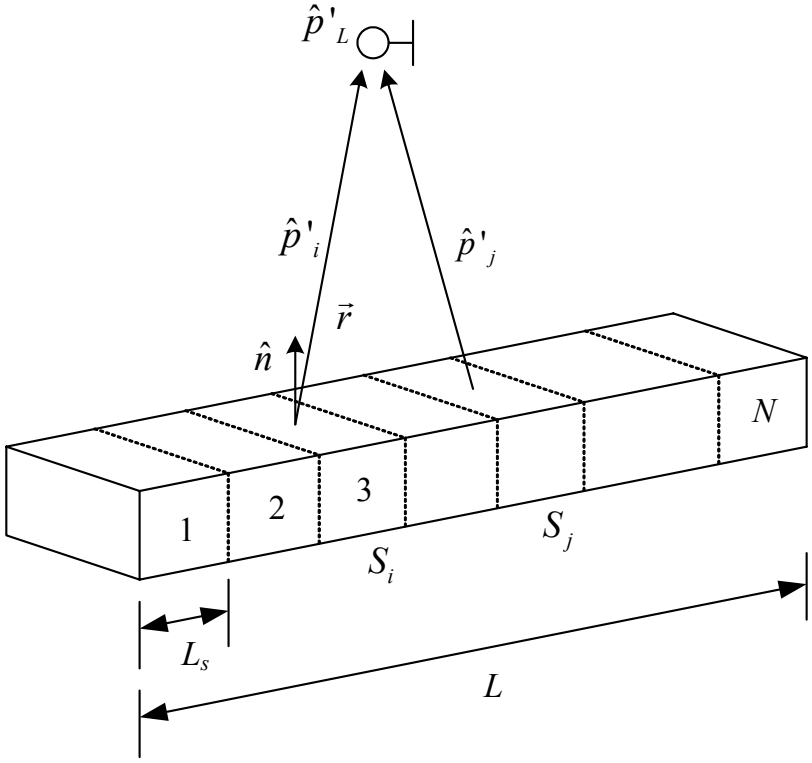

Fig. 1 Schematic of a long-span body divided into *N* subsections.

where r is a distance from the source to the observer's position, $\hat{n}$ is a unit vector normal to the Kirchhoff surface, and H is the Hankel function. In Eq. (10), the effect of momentum fluctuations (Lighthill stress tensor) is neglected, because the Kirchhoff surface is set in the mid-field, along which the momentum fluctuations are usually negligible.

C. Estimation of Far-Field SPL for Long Span

In order to estimate the sound pressure level (SPL) for the long span (L), SPL for the simulated span (L_s) must be corrected. According to Kato et al.[21], the SPL for long span can be obtained by adding $10\log(L/L_s)$, if a coherence length of the surface pressure fluctuation L_C is determined as $L_C \le L_s$. If $L_C > L$, $20\log(L/L_s)$ must be added to the SPL for the simulated span. Asymptotic behaviors at two ends are correct but Kato's approach is rather *ad hoc,* when $L_s \le L_C \le L$. This simple correction method has been employed in various studies[1,7,17,22]. Recently, Perot et al.[2] proposed a correction method, considering an acoustic spanwise coherence function with Curle's analogy solution. The method gives a more realistic result in the near-field because a retarded time is taken into account but has not been completed for practical use.

In this study, we propose a method, extending the Perot's work on the base of Kato's. First, consider a long-span body divided by N subsections with L_s (i.e. $L=N\cdot L_s$) because acoustic pressure radiated from the simulated span, L_s is the only known solution (see Fig. 1). Let the spectral acoustic pressure radiated from the i-th subsection be $\hat{p}'_i$, then the power spectral density of the acoustic pressure for the entire span, $\hat{p}'_L$ can be obtained by

$$\hat{p}'_L \, \hat{p}'^{*}_L = \sum_{i=1}^{N} \hat{p}'_i \cdot \sum_{j=1}^{N} p'^{*}_j = \sum_{i=1}^{N} \sum_{j=1}^{N} \mathrm{Re}(\hat{p}'_i \, \hat{p}'^{*}_j), \tag{11}$$

where * denotes a conjugate. Now, we need an assumption of '*statistical homogeneity in the spanwise direction*' that satisfies the following properties. For a proper L_s,

1. The power spectral density of the acoustic pressure radiated from each subsection is the same, i.e.

$$\left|\hat{p}'_1\right|^2 = \left|\hat{p}'_2\right|^2 = \quad ..... \quad = \left|\hat{p}'_N\right|^2 = \left|\hat{p}'_s\right|^2, \tag{12}$$

where $\hat{p}'_s$ is the spectral acoustic pressure radiated from the span, L_s.

2. The acoustic pressure radiated from each subsection is only lagged by a phase difference which can be characterized by the following coherence function,

$$\gamma'_{ij} = \frac{\overline{\mathrm{Re}(\hat{p}'_i\,\hat{p}'^{*}_j)}}{\sqrt{\left|\hat{p}'_i\right|^2}\sqrt{\left|\hat{p}'_j\right|^2}}. \tag{13}$$

One must note that this coherence function is different from the coherence of the far-field acoustic pressures at two locations separated in the spanwise direction.

3. The above coherence function (phase lagging) is a function of Δz_{ij}, the spanwise separation between the two subsections:

$$\gamma'_{ij} = \gamma'(\Delta z_{ij}), \qquad \Delta z_{ij} = \left|z_i - z_j\right| = \left|i-j\right| \cdot L_s. \tag{14}$$

In most of turbulent flows around long-span bodies, these assumptions are not so crude, if the observer's position is very far. Applying Eqs. (12)-(14), Eq. (11) can be re-written as

$$\left|\hat{p}'_L\right|^2 = \sum_{i=1}^{N}\sum_{j=1}^{N} \gamma'(\Delta z_{ij}) \cdot \left|\hat{p}'_s\right|^2, \tag{15}$$

where $\hat{p}'_s$ is our known solution, i.e. acoustic pressure radiated from the simulated span, L_s.
So, we can now estimate the acoustic pressure for the long span by determining $\gamma'(\Delta z_{ij})$. Since the phase lagging in the spanwise direction tends to follow a Gaussian distribution[25,26], $\gamma'(\Delta z_{ij})$ can be expressed as

$$\gamma'(\Delta z_{ij}) = \exp\left(-\frac{\Delta z_{ij}^{\,2}}{L'_c(\omega)^2}\right), \tag{16}$$

where L'_c is the spanwise coherence length which is also a function of frequency.

From Eqs. (15) and (16), SPL(*dB*) to be corrected for the long span, *L* is given by

$$SPL_c(\omega) = 10\log\left(\frac{\left|\hat{p}'_L(\omega)\right|^2}{\left|\hat{p}'_s(\omega)\right|^2}\right) = 10\log\left(\sum_{i=1}^{N}\sum_{j=1}^{N}\exp\left(-(i-j)^2\left(\frac{L_s}{L'_c(\omega)}\right)^2\right)\right). \tag{17}$$

The SPL_c is plotted in Fig. 2 (solid line) against L'_c/L_s for various $N(=L/L_s)$. If $L'_c/L_s < 1/\sqrt{\pi}$ (≈ 0.56), SPL_c converges to $10\log(N)$, while $SPL_c \to 20\log(N)$ for $L'_c > L$. When N is sufficiently large, SPL_c is linearly proportional to $\log(L'_c/L_s)$ in the range of $1/\sqrt{\pi} < L'_c/L_s < N/\sqrt{\pi}$ and therefore Eq. (17) can be approximated to a more simple form (dashed line), which might be useful in an engineering purpose:

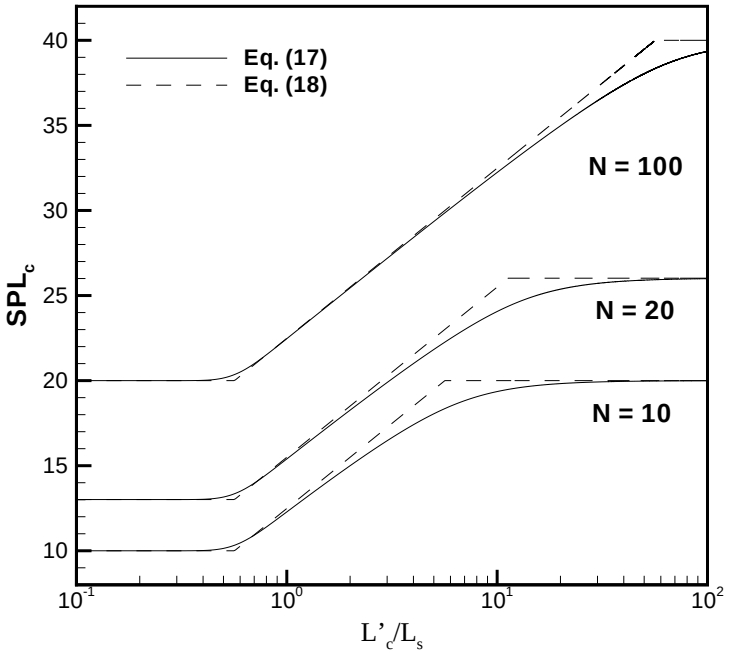

Fig. 2 SPL to be added for long span.

$$SPL_c = \begin{cases} 10\log(N) & L'_c / L_s \le 1/\sqrt{\pi} \ (\approx 0.56) \\ 10\log(L'_c / L_s) + 10\log(\sqrt{\pi}\, N) & 1/\sqrt{\pi} < L'_c / L_s < N/\sqrt{\pi} \\ 20\log(N) & L'_c / L_s \ge N/\sqrt{\pi} \end{cases} . \tag{18}$$

One can see that Eq. (17) or (18) has the same asymptotic behavior as Kato's formula and also that Eq. (18) is still useful for small *N,* as long as L'_c / L_s is not so large (less than 3, for example).

As shown above, determining L'_c from the spanwise coherence function $\gamma'(\Delta z_{ij})$ is crucial for estimation of the SPL to be added for long span. Actually, $\gamma'(\Delta z_{ij})$ is the spanwise coherence function between the acoustic pressures radiated from each subsections but experimentally measuring that is hardly possible because the acoustic far-field cannot be windowed (or sectioned) by L_s for the entire span. Alternatively, the function can be estimated by an acoustic analogy with the simulated (or measured) surface pressure data[2]. The cross power spectrum $\hat{p}'_i \hat{p}'^*_j$ can be evaluated from the surface pressure, using the Curle's solution:

$$\hat{p}'(\omega) \simeq \frac{1}{4\pi c_0} \int (\vec{r} \cdot \hat{n})(-i\omega \hat{P}(\omega)) \exp(i\omega r / c_0)\, dS . \tag{19}$$

For a compact source and when the observer's position is very far, it can be assumed that $r / c_0 \approx (const.)$. The cross power spectrum $\hat{p}'_i \hat{p}'^*_j$ is then analytically written as

$$\hat{p}'_i \hat{p}'^*_j \simeq \left| \frac{-i\omega \exp(i\omega r / c_0)}{4\pi c_0} \right|^2 \int (\vec{r} \cdot \hat{n}) \hat{P}_i \, dS_i \cdot \int (\vec{r} \cdot \hat{n}) \hat{P}^*_j \, dS_j , \tag{20}$$

and then Eq. (13) becomes

$$\gamma'_{ij} \simeq \frac{\overline{\mathrm{Re}\left(\int (\vec{r}\cdot\hat{n})\ \hat{P}_i\ dS_i \cdot \int (\vec{r}\cdot\hat{n})\ \hat{P}_j^{*}\ dS_j\right)}}{\sqrt{\left|\int (\vec{r}\cdot\hat{n})\,\hat{P}_i\,dS_i\right|^2}\sqrt{\left|\int (\vec{r}\cdot\hat{n})\,\hat{P}_j\,dS_j\right|^2}}\ , \tag{21}$$

where $\hat{P}_i$ is the surface pressure at each subsection and $\int dS_i$ is the surface integral over each subsectional area. Equation (21) expresses the spanwise coherence function $\gamma'(\Delta z_{ij})$ in terms of the 'integrated' surface pressures. For a certain flow, it is also possible to replace $\gamma'(\Delta z_{ij})$ by the spanwise coherence function of the surface pressure at a particular point of interest. Such a coherence function can be easily measured in experiments.

III. Results and Discussion

In order to validate the present computational methodologies, we consider a flow-induced noise from a circular cylinder with 30*D* span. A schematic is shown in Fig. 3. This cylinder cross-flow is at Re_D=4.6×10^4 (and M=0.21), which is in a a sub-critical regime (1×10^3 <Re_D <2×10^5) and generates a broadened dipole-tone due to the von Karman vortex shedding as well as the broadband components induced by wake turbulences. Its aerodynamic coefficients, *St,* C_L and C_D in *rms* and averaged values have been measured by Szepessy & Bearman[23], while the acoustic measurements were recently conducted at *Ecole Centrale de Lyon*[1,26]. The present case is considered as a benchmarking problem for the prediction of a low Mach number turbulent flow noise radiated from a long-span body.

A. Turbulent Flow around a Circular Cylinder

At Re_D=46000, a laminar boundary layer on the cylinder surface separates and the shear layer immediately transits to turbulences. According to Szepessy[24], who measured the spanwise integral correlation length as L_c=2.7*D* at Re_D=43000, an incompressible LES was conducted for a spanwise width, L_s=3*D* (see Fig. 3) with a flow periodicity assumed in the spanwise direction. An O-type cylindrical grid is used with approximately 10^6 points: 181 for the circumferential and radial directions and 31 for the spanwise (*z*) direction. The computational domain is divided into 16 blocks for parallel computation.

After about 100 non-dimensional time (100*tU/D*), a pseudo periodic-stage is established. An additional computation was conducted for 200 non-dimensional time, obtaining 80 cycles of von Karman vortex shedding. Iso-surfaces of the second invariant property of the velocity gradient, *Q* defined as

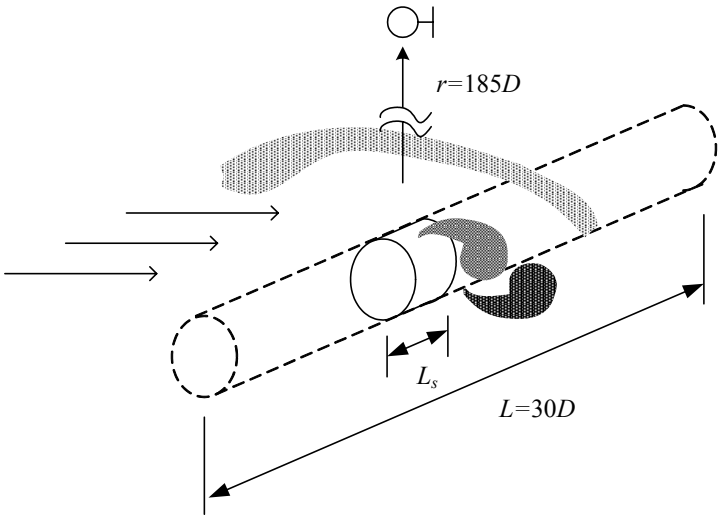

Fig. 3 Schematic of a long circular cylinder in cross flow.

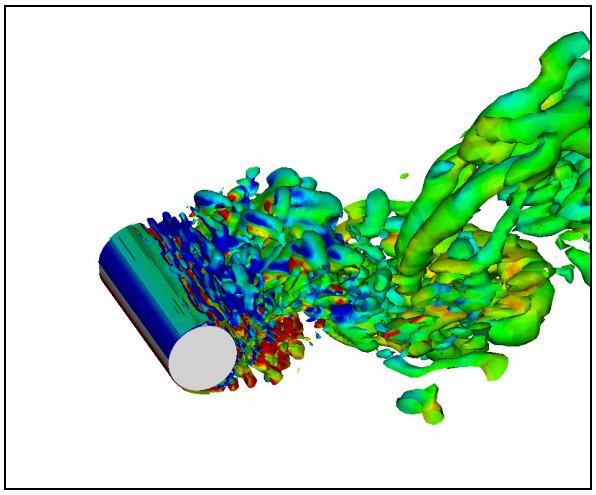

Fig. 4 Three-dimensional vortical structure around a circular cylinder at Re_D=46000 and M=0.21; Iso-surface of Q=0.5, non-dimensionalized by $(U_\infty/D)^2$.

$$Q = (\Omega_{ij}\Omega_{ij} - S_{ij}S_{ij})/2,$$
$$S_{ij} = \frac{1}{2}\left(\frac{\partial U_i}{\partial x_j} + \frac{\partial U_j}{\partial x_i}\right) \text{ and } \Omega_{ij} = \frac{1}{2}\left(\frac{\partial U_i}{\partial x_j} - \frac{\partial U_j}{\partial x_i}\right) \quad (22)$$

are plotted in Fig. 4. It shows highly three-dimensional wake structures around the circular cylinder as well as the coherent von Karman vortex streets. The boundary layer at the cylinder surface remains laminar before separation but the shear layers immediately break off into eddies and transits to turbulences. In the rear part of the cylinder as well as in the wake, complicated three-dimensional eddy structures are shown. The time variations of the drag and lift coefficients are shown in Fig. 5(a). The lift coefficient oscillates at the von Karman vortex shedding frequency (St=0.19), while the drag coefficient exhibits less periodic oscillations at St=0.38. The mean pressure coefficient at the cylinder surface is also compared in Fig. 5(b) with the experimental data[23], indicating a fairly good agreement. The back pressure and the lowest peak are slightly under-predicted but the position of the lowest peak seems to be well met.

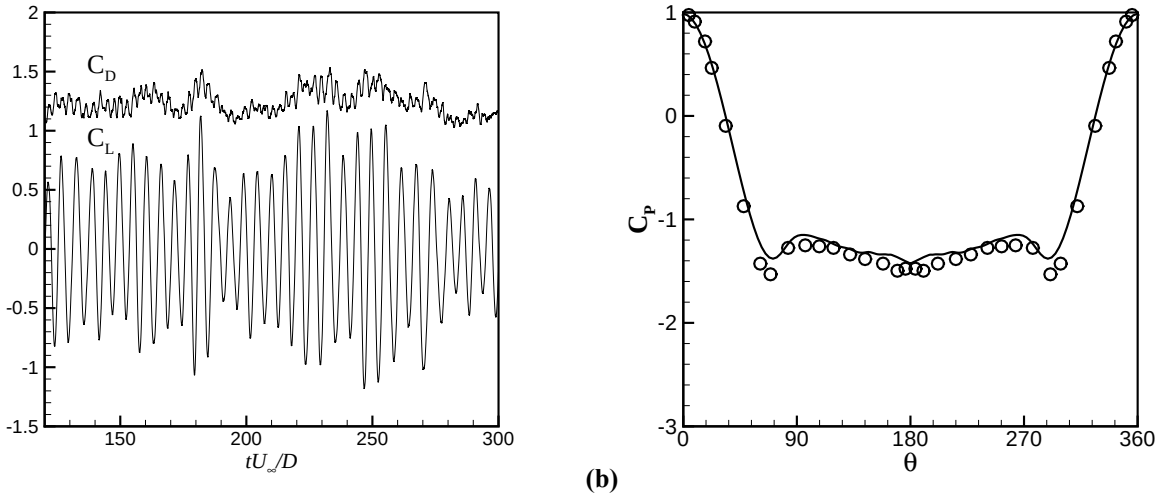

(a) **(b)**

Fig. 5 Aerodynamic characteristics; (a) time variations of the drag and lift coefficients, (b) mean pressure coefficient around the cylinder; — : present computation, o : measurement (Szeppsy and Bearman).

Table 1 Aerodynamic coefficients

	St	$C_{D,avg}$	$C_{D,rms}$	$C_{L,rms}$
Present	0.187	1.24	0.1	0.54
Experiment	0.19	1.35	0.16	0.45-0.5

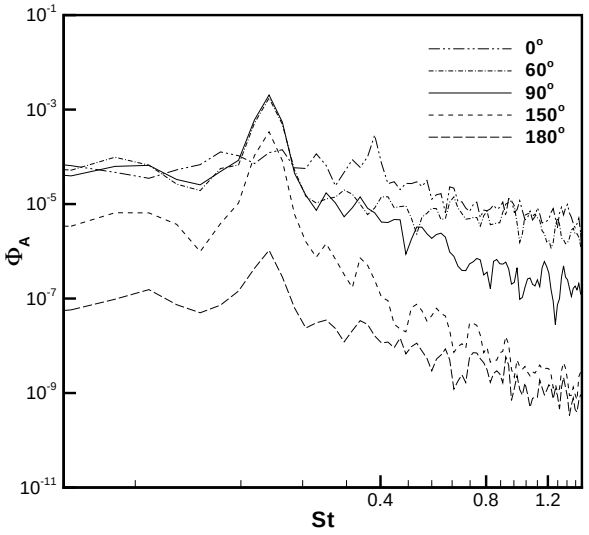

Fig. 6 Auto-spectra of surface pressure fluctuation over the cylinder.

The aerodynamic coefficients summarized in Table 1 are compared with the experimental data of Szepessy & Bearman[23]. The computed Strouhal number ($St=fD/U$) agrees well with the experimental value. The drag coefficient in *rms* value is slightly under-predicted but the mean drag coefficient and *rms* value of the lift coefficient are in good agreement. The discrepancy in numerical result may be caused by the limitation of the spanwise simulation width or absence of the sub-grid scale model.

In Fig. 6, auto-spectra of the surface pressure fluctuations, $\Phi_A(\omega) = \hat{P}(\omega)\hat{P}^*(\omega)$ over the cylinder are plotted for various circumferential positions (θ=0° corresponds to the wake line). The main peak at St=0.19 is observed in every position except at the wake line, where a peak at St=0.38 is more pronounced due to the alternate vortex shedding. The maximum peak at St=0.19 is observed at θ=90° (cylinder top position), as expected. The strength of the pressure fluctuations at St >0.3 is higher at the cylinder rear positions, due to the turbulent fluctuations in the wake region. Figure 7(a) also shows the auto-spectra of the pressure fluctuations at θ=90° along the spanwise direction, while the spanwise phase difference, $\Delta\phi = \arctan(\mathrm{Im}(\Phi_C)/\mathrm{Re}(\Phi_C))$ is presented in Fig. 7(b), where $\Phi_C = \hat{P}(\omega, z)\hat{P}^*(\omega, z+\Delta z)$ is the cross spectra of the surface pressure fluctuations at θ=90°. The phase difference is evaluated with 10 ensemble-averages, which may not be sufficient to obtain an accurate value but a tendency is clearly illustrated. As one can see, the auto-spectra are almost identical in the spanwise direction, while the phase difference is increasing with the spanwise separation. The variation of the phase difference becomes larger as the frequency increases. From these results, a flow over the circular cylinder may be regarded as *statically homogenous in the spanwise direction*.

B. Acoustic Field Computation (LPCE)

In order to apply the methodology described in Sec. II-B, a 2D LPCE computation is conducted with the incompressible LES solution spanwise-integrated at the zero spanwise wave number, k_z=0, i.e.

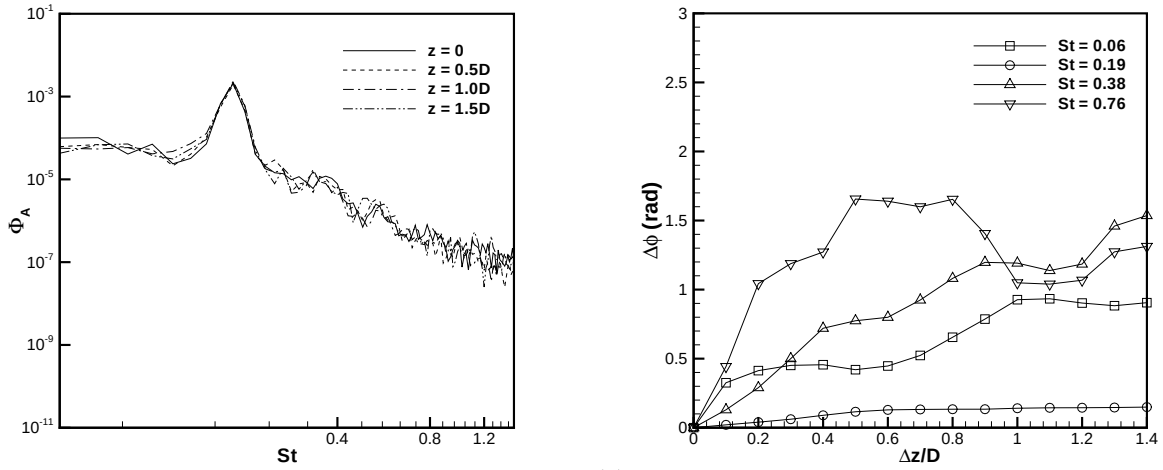

(a) **(b)**

Fig. 7 Spanwise spectral characteristics; (a) Auto-spectra of the surface pressure fluctuation (b) Phase difference determined from the cross-spectra.

$$U(x,y) = \int_0^{L_s} \tilde{U}(x,y,z)dz\,. \tag{23}$$

The acoustic grid composed of 161×241 points are distributed over a computational domain radially extended to r=80D. In this problem, an acoustic wavelength at the Karman vortex shedding frequency, St=0.19 is expected to be about 25D at M_∞=0.2 and the grid distribution is designed to resolve this sound wave with 40 grid points in the mid-field (i.e. r~50D). The minimal grid spacing of the acoustic grid at the wall is five times larger than the hydrodynamic grid so that acoustic calculation can be conducted with the same time step used for the incompressible LES. This is one of the advantages of the hydrodynamic/acoustic splitting method[13]. The spanwise-integrated incompressible LES solution is directly interpolated onto the acoustic grid using a bi-linear shape function.

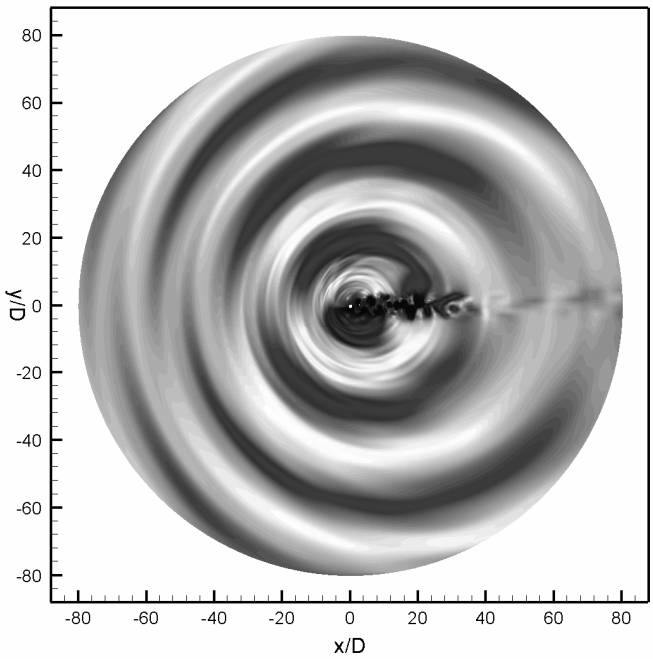

Fig. 8 Instantaneous pressure fluctuation field over the cylinder (Re_D=46000 and M_∞=0.21).

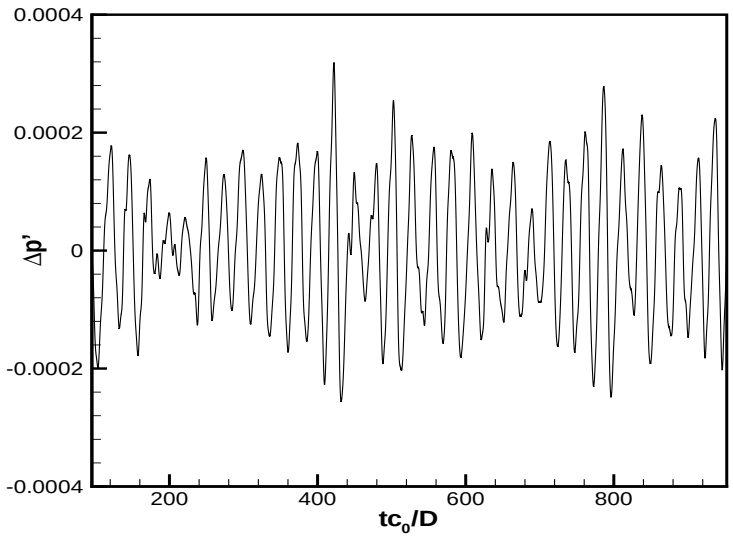

Fig. 9 Time variation of pressure fluctuating at r=70D directly above the cylinder, non-dimensionalized by $\rho_\infty c_\infty^2$.

Figure 8 shows an instantaneous pressure fluctuation field ($\Delta p' = \overline{(P+p')} - (P+p')$) calculated by LPCE for the entire acoustic domain. One can see the dominant acoustic waves (tonal) as well as other high frequency waves in the near field. The dipole tone is generated by the coherent Karman vortex shedding, while the short-wavelength waves are emanated from the volume sources (i.e. shear layer breaking-off and wake turbulences). A time variation of the pressure fluctuations at r=70D directly above the cylinder is presented in Fig. 9. Acoustic pressure oscillates at a dominant vortex shedding frequency but not regular as compared with the laminar tone[13]. Therefore, directivity of $\Delta p'_{rms}$ at r=70D presented in Fig. 10 indicates the dipole characteristics but the directivity pattern is not like the laminar case (i.e. twin circles).

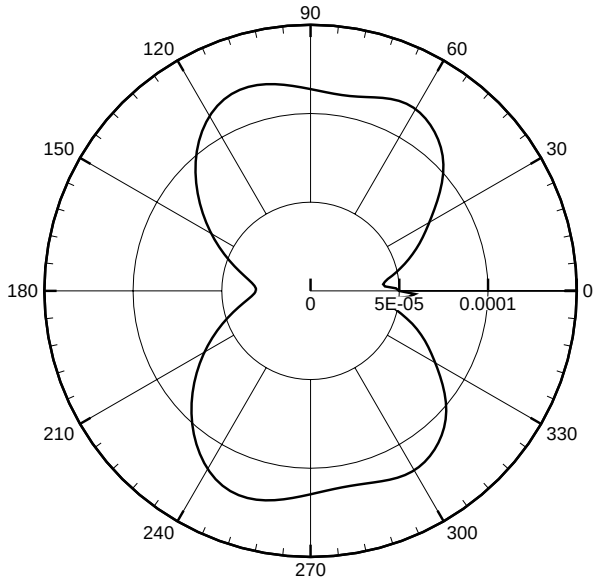

Fig. 10 Directivity pattern of $\Delta p'_{rms}$ at r=70D, non-dimensionalized by $\rho_\infty c_\infty^2$.

C. Estimation of far-field SPL for Long Span

As shown in Fig. 3, the sound pressure level in the experiment was measured at r=185D away from the cylinder, while the acoustic domain only extends up to r=80D. Therefore, the acoustic pressure at r=70D (i.e. the Kirchhoff surface) needs to be extrapolated to r=185D by a 2D Kirchhoff method, Eq. (10) and then followed by a 3D spectral acoustic pressure correction with Oberai's formula, Eq. (9).

In order to verify the computational methods, the power spectral density (PSD) of the acoustic pressure at r=185D computed by LPCE with Eqs. (9) and (10) is compared in Fig. 11 with the Curle's analogy solution, considering only the surface sources. The SPL spectra are quite similar, in overall, including the match of the peak at St~0.19. Some discrepancy found in the high frequency region (e.g. 0.3<St<1.2) is due to the fact that the volume sources in the wake region were not represented in the Curle's solution. The LPCE result, however, well shows the corresponding attributions, i.e. the spectrum level increase in that region, including two clear peaks at St~0.38 and 0.56 (also confirmed in the experimental data, see Fig. 14).

In order to estimate the far-field SPL for the actual span (L=30D), a correction must be taken into account to the SPL for the simulated span (L_s=3D) by Eq. (17) (or (18)) with consideration of a coherence function, $\gamma'(\Delta z)$. In the present study, the coherence function can be calculated by dividing the spanwise width, Δz=L_s into 30 smaller subsections and applying the Curle's analogy to each subsection (i.e. 0.1D). The calculated coherence function (symbols in Fig. 12) is, however, only valid up to $\Delta z = L_s/2$=1.5D because a periodic boundary condition was used in the spanwise direction. Except at the vortex shedding frequency (St=0.19), the coherence functions at other frequencies are rapidly decaying, as Δz increases. One can easily fit them with a Gaussian function $\exp(-\Delta z^2/ L'^2_c)$ (solid line in Fig. 12) and determine the coherence length L'_c for each frequency. Around the vortex shedding frequency, the coherence function is so slowly decaying that a fitting may yield an inaccurate estimation of L'_c, although its sensitivity to the SPL is found rather weak. More discussion will follow later in this section.

In the present study, we invoke a use of the experimentally measured coherence (or correlation). Since the experimental measurement of coherence is only made for the surface pressure[25,26], it would be useful to replace γ'_{ij} by the coherence function of the surface pressure. The coherence function γ' is related to the integrated surface pressure, as described in Eq. (21). In the present problem, the integrated surface pressure in Eq. (21) is dominated by the surface pressure fluctuations at the cylinder top (θ=90°) because the directional cosine ($\vec{r}\cdot\hat{n}$) and the surface pressure fluctuations as well have a peak at this position (see Figs. 3 and 6). The coherence function of the surface pressure fluctuation at θ=90°, Γ is given by

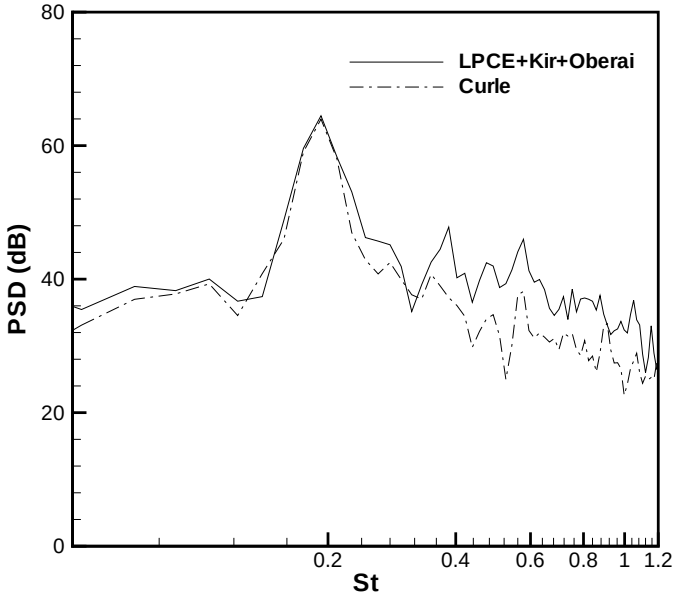

Fig. 11 PSD of acoustic pressure at r=185D directly above the cylinder for span, L_s (=3D).

$$\Gamma_{ij}(\omega) = \frac{\overline{\mathrm{Re}(\hat{P}_i(\omega)\hat{P}_j^*(\omega))}}{\sqrt{\left|\hat{P}_i(\omega)\right|^2}\sqrt{\left|\hat{P}_j(\omega)\right|^2}}\ , \tag{24}$$

where the subscript denote a subsection of the span. The coherence function of the surface pressure fluctuation calculated at θ=90° is presented in Fig. 13 (symbols) and also fitted with the Gaussian function (solid line). At the vortex shedding frequency, the computation yields a coherence length, 6*D,* which well coincides with the experimentally measured value[25,26]. As one can see in Fig. 12 and 13, the spanwise coherence functions, γ' and Γ at θ=90° are quite similar and in practice, γ' can be replaced by the surface pressure coherence function Γ at a proper position. The coherence function, Γ is often available in the experimental measurement or can be easily computed

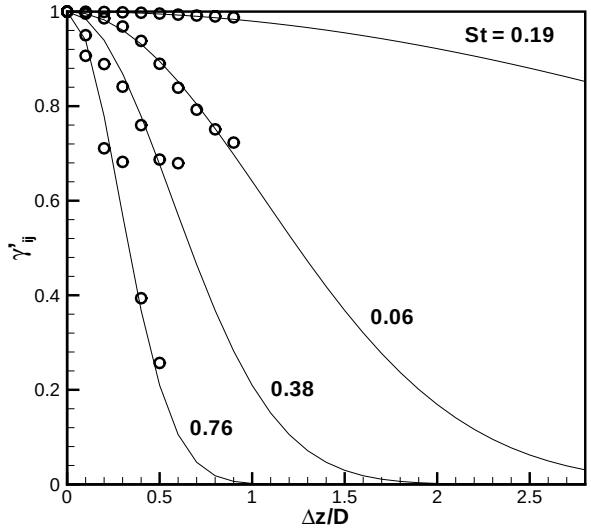

Fig. 12 Spanwise coherence function of the acoustic pressures emitted from the simulated span.

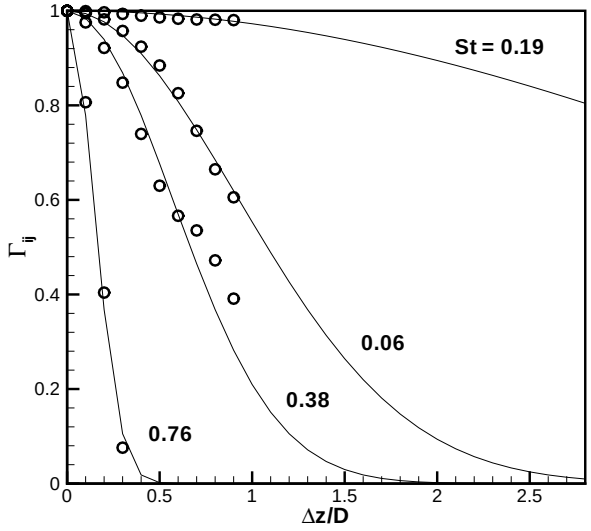

Fig. 13 Spanwise coherence function of the surface pressure over the simulated span (θ=90°).

Table 2 Calculated spanwise coherence length

St		**0.06**	**0.19**	**0.38**	**0.76**
$L'_c(\omega)$	γ'	1.5D	7D	0.8D	0.4D
	Γ	1.3D	6D	0.8D	0.2D

from the simulation (if the simulated span is long enough). Actually, the surface pressure coherence is not perfectly the same as the acoustic coherence because it depends on the position and is also problem-dependent. So, the coherence length determined by the surface pressure coherence may be slightly different form that obtained by the acoustic coherence. The amount of SPL to be added for long span is, however, not so sensitive to the accuracy of the coherence length.

The coherence lengths L'_c determined from Figs. 12 and 13 are listed in Table 2. They are found slightly different. At St=0.76, the coherence length for the surface pressure is smaller by half than that of the acoustic pressure. It is because the high frequency fluctuations are not substantially noticeable at θ=90° (see Fig. 3). The differences at other frequencies are also not so significant. For most of the frequencies except at Karman vortex shedding, coherence lengths are smaller than $L_s/\sqrt{\pi} \approx 1.7D$ and according to Eq. (18), $SPL_c = 10\log(N) = 10$ (dB) should be added to obtain the SPL for the long span. In fact, obtaining a precise value of L'_c is not so crucial for those frequencies. It is interesting to note that the frequencies around St=0.19 (vortex shedding frequency) fall into the case of $1/\sqrt{\pi} < L'_c/L_s < N/\sqrt{\pi}$. Since the coherence length is larger than the simulated span, the calculated coherence length could be inaccurate. For the present case (i.e. N=10, L_s=3D and $L'_c \sim 6D$), however, ±1D variation in L'_c corresponds to ±1 (dB) in SPL_c. Therefore, a reasonable estimation of coherence length may suffice the case. In this regard, a difference in coherence lengths determined by γ' and Γ makes only small influence to the final SPL (up to 1dB).

The far-field SPL for L=30D is then estimated by Eq. (17) with the coherence lengths listed in Table 2 (with γ'). The acoustic pressure PSD is compared in Fig. 14 with the measured data of *Ecole Centrale de Lyon*[1,26]. The computed SPL spectrum agrees well with the experimental data, including the main and secondary peaks. Furthermore, the broadening of the peak around the Karman vortex shedding frequency also closely matches with

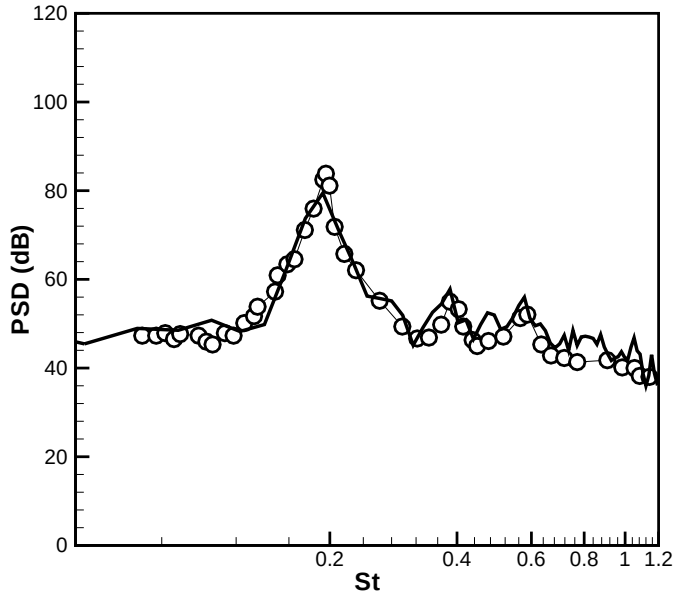

Fig. 14 Sound pressure level spectrum at r=185D for L=30D; — : present, O: measurement[1,26].

the experiment. The high-frequency region also well coincides with the measured one. From this comparison, it is shown that the present methodology is consistent and capable of predicting a low Mach number turbulent flow noise for long-span bodies.

IV. Conclusive Remarks

An aerodynamic noise prediction method for long-span bodies is proposed, especially for the turbulent flow noise at low Mach numbers. Accuracy of the present method is assessed for a broadened tone as well as the broadband noise generated by a flow (Re_D=4.6×10^4 and M=0.21) past a circular cylinder with 30D span. The aerodynamic coefficients, St, C_L and C_D in *rms* and averaged values computed by incompressible LES for short span are closely compared with the experimentally measured data, showing a statistical spanwise homogeneity of the flow.

The far-field sound pressure level for the long span is calculated by an approximate but efficient computational procedure:

(1) A two-dimensional acoustic near- and mid-field is computed by LPCE with the spanwise-integrated incompressible LES solution.
(2) Acoustic pressure in the far field is obtained by extrapolating the mid-field solution with the Kirchhoff method.
(3) A three-dimensional correction of the spectral acoustic pressure is made by Oberai's formula.
(4) Finally, the sound pressure level for the simulated span is corrected to that for the long span, considering the spanwise coherence function of the surface pressure.

The solution procedures from (1) to (3) are validated by the Curle's acoustic analogy solution. The step (4), i.e. correction of the far-field SPL for the long span is formally derived by considering a spanwise coherence of the acoustic pressures emitted from each subsection along the long-span body and also shown to be quite accurate, in comparison with the experimentally measured far-field SPL. With the spanwise coherence length determined by a Gaussian law, it is numerically shown that the spanwise coherence function of the acoustic pressure is not too different from that of the surface pressure at a particular point of our interest and that the SPL to be corrected for the long span is not too sensitive to the spanwise coherence length determined computationally.

References

[1]Boudet, J., Casalino, D., Jacob, M. C., and Ferrand, P., "Prediction of Sound Radiated by A Rod Using Large Eddy Simulation," AIAA-Paper 2003-3217, 2003.

[2]Perot, F., Auger, J. M., Giardi, H., Gloerfelt, X., and Baily, C., "Numerical Prediction of the Noise Radiated by a Cylinder," AIAA-Paper 2003-3240, 2003.

[3]Gloerfelt, X., Bogey, C., and Baily, C., "LES of the Noise Radiated by a Flow over a Rectangular Cavity," *Proceedings of LES for Acoustics*, DGLR-Report 2002-03, 2002.

[4]Terracol, M., Manoha, E., Herrero, C., and Sagaut, P., "Airfoil Noise Prediction using Large Eddy Simulation, Euler Equation and Kirchhof Integral," *Proceedings of LES for Acoustics*, DGLR-Report 2002-03, 2002.

[5]Baily, C., and Bogey, C., and Juve, D., "Computation of Flow Noise using Source Terms in Linearized Euler Equaions," AIAA-Paper 2000-2047, 2000.

[6]Ewert, R., and Schröder, W., "Acoustic Perturbation Equations Based on Flow Decomposition via Source Filtering," *Journal of Computational Physics*, Vol. 188, 2003, pp. 365-398.

[7]Ewert, R., and Schroder, W., "On the Simulation of Trailing Edge Noise with a Hybrid LES/APE Method," *Journal of Sound and Vibration*, Vol. 270, 2004, pp. 509-524.

[8]Hardin, J. C., and Pope, D. S., "An Acoustic/Viscous Splitting Technique for Computational Aeroacoustics," *Theoret. Comput. Fluid Dynamics*, Vol. 6, 1994, pp. 323-340.

[9]Shen, W. Z., and Sorenson, J. N., "Aeroacoustics Modeling of Low-speed Flow," *Theoret. Comput. Fluid Dynamics*, Vol. 13, 1999, pp. 1057-1064.

[10]Shen, W. Z., and Sorenson, J. N., "Aeroacoustic Modeling of Turbulent Airfoil Flows," *AIAA Journal*, Vol. 39, No. 6, 2001, pp. 1057-1064.

[11]Slimon, S. A., Soteriou, M. C., and Davis, D. W., "Computational Aeroacoustics Simulations Using the Expansion about Incompressible Flow Approach," *AIAA Journal*, Vol. 37, No. 4, 2000, pp. 409-416.

[12]Slimon, S. A., Soteriou, M. C., and Davis, D. W., "Development of Computational Aeroacoustics Equations for Subsonic Flows Using a Mach Number Expansion Approach," *Journal of Computational Physics*, Vol. 159, 2000, pp. 377-406.

[13]Seo, J. H., and Moon, Y. J., "The Perturbed Compressible Equations for Aeroacoustic Noise Prediction at Low Mach Numbers," *AIAA Journal*, Vol. 43, No. 8, pp. 1716-1724, 2005.

[14]Seo, J. H., and Moon, Y. J., "Linearized Perturbed Compressible Equations for Low Mach Number Aeroacoustics," *Journal of Computational Physics* (accepted for publication), 2006.

[15]Lele, S. K., "Compact Finite Difference Schemes with Spectral-like Resolution," *Journal of Computational Physics*, Vol. 103, 1992, pp. 16-42

[16]Gaitonde, D., Shang, J. S., and Young, J. L., "Practical Aspects of Higher-Order Numerical Schemes for Wave Propagation Phenomena," *International Journal for Numerical Methods in Engineering*, Vol. 45, No. 12, 1999, pp. 1849-1869.

[17]Manoha, E., Delahay, C., Sagaut, P., Mary, I., Khelil, S., and Guillen, P., "Numerical Prediction of Unsteady Flow and Radiated Noise from a 3D Lifting Airfoil," AIAA-Paper 2001-2133, 2001.

[18]Seo, J. H., and Moon, Y. J., "Prediction of Low Mach Number Turbulent Flow Noise Using The Splitting Method, " AIAA-Paper 2004-2860, 2004.

[19]Oberai, A. A., Roknaldin, F., and Hughes, T. J. R., "Trailing-Edge Noise Due to Turbulent Flows," Technical Report, Boston University, Report No. 02-002, 2002.

[20]Scott, J. N., Pilon, A. R., Lyrintzis, A. S., and Rozmajzl, T. J., "A Numerical Investigation of Noise From a Rectangular Jet," AIAA-Paper 1997-285, 1997.

[21]Kato, C., Iida, A., Takano, Y., Fujita, H., and Ikegawa, M., "Numerical Prediction of Aerodynamic Noise Radiated from Low Mach Number Turbulent Wake," AIAA-Paper 93-145, 1993.

[22]Ewert, R., Meinke, M., and Schroder, W., "Computation of Trailing Edge Noise of a 3D Lifting Airfoil in Turbulent Subsonic Flow," AIAA-Paper 2003-3114, 2003.

[23]Szepessy, S., and Bearman, P. W., "Aspect Ratio and End Plate Effect on Vortex Shedding from a Circular Cylinder," *Journal of Fluid Mechanics*, Vol. 234, 1992, pp. 191-217.

[24]Szepessy, S., "On the Spanwise Correlation of Vortex Shedding from a Circular Cylinder at High Subcritical Reynolds Number," *Physics of Fluid*, Vol. 6, No. 7, 1994. pp. 2406-2416.

[25]Casalino, D., and Jacob, M., "Prediction of Aerodynamic Sound from Circular Rods via Spanwise Statistical Modelling," *Journal of Sound and Vibration*, Vol. 262, No. 4, 2003, pp. 815-844.

[26]Jacob, M. C., Boudet, J., Casalino, D., and Michard, M., "A Rod-Airfoil Experiments as a Benchmark for Broadband noise modeling," *Theoret. Comput. Fluid Dynamics*, Vol. 19, No. 3, 2005, pp. 171-196.